Implementation of a Constitutive Model for Aluminum Foam Including Fracture and Statistical Variation of Density

A. Reyes, O. S. Hopperstad, T. Berstad, and M. Langseth
Structural Impact Laboratory (SIMLab), Department of Structural Engineering,
Norwegian University of Science and Technology
Rich. Birkelands vei 1A, N- 7491 Trondheim, Norway

Abstract

An existing constitutive model applicable to aluminum foam was implemented in LS-DYNA. One main objective in the present project was to implement a model that could handle fracture in the foam. Therefore, two simple fracture criteria were also implemented in the model. Additionally, the possibility to include initial statistical variation of the foam density was incorporated in the model so that inhomogeneities in the foam properties could be represented. Foam subjected to both simple and more complex loading conditions where fracture was of varying importance have been analyzed, and some representative results and comparisons with experimental data are presented. The implemented model is efficient and robust, and gives good results. The model including one of the fracture criteria and without the possibility of statistical variation of density is at present available in version 970 of LS-DYNA.

Introduction

Energy absorbers are often used in cars, trains, buses etc. to protect passengers and the structure during impact. Due to its excellent energy-absorbing capability, aluminum foam may be used in such devices. As vehicle design requires numerical simulations by finite element programs such as LS-DYNA (Hallquist 1998), it is important to have good constitutive models also for foams. Hanssen et al. (2002) concluded that the different models for metallic foams available in LS-DYNA in 2002 were not able to predict the behavior of different experimental verification tests. One of the reasons for the discrepancy between experimental and numerical results was the lack of a suitable fracture criterion.

Several challenges exist in the material modeling of foam since it is a cellular material. Contrary to metals, which sustain the same volume when loaded, the volume changes for foams during loading. The material model should therefore include the possibility of failure under hydrostatic loading conditions. Another important characteristic of aluminum foam is the inhomogeneity of the pores, which are of different sizes and are not distributed evenly. A few approaches to model the inhomogeneities of foam can be found in the literature (Daxner et al. 1999, Gradinger and Rammerstorfer 1999, Meguid et al. 2002).

Several constitutive models for foams exist in the literature (Schreyer et al. 1994, Zhang et al. 1997, Ehlers 1999, Deshpande and Fleck 2000, Miller 2000). Some of them are quite simple; others are more complicated with several material parameters. There are also few or no recommendations on how to include the uneven distribution of pores and fracture in the models.

The yield criterion presented by Deshpande and Fleck (2000) can be regarded as an extension of the von Mises yield criterion, where the hydrostatic stresses are incorporated in the equivalent

stress. Because of its simplicity, the Deshpande-Fleck model was chosen for implementation in LS-DYNA. Furthermore, it was decided to incorporate initial statistical variation of density and different fracture criteria. Two simple fracture criteria were added to the model, and including an initial statistical variation of foam density enabled modeling of inhomogeneities in the foam.

The main objective of the current paper is to present the model (Section 2) and the implementation procedure (Section 3) in detail. Section 4 and 5 describes shortly how statistical variation of density and fracture was included. Several numerical analyses of verification tests on Hydro aluminum foam has been performed and compared with experimental results from Hanssen et al. (2002). The results from these tests have been reported by Reyes et al. (2003), but some of the findings are presented in Section 6 of the present paper.

Constitutive Model

The constitutive model presented by Deshpande and Fleck (2000) is isotropic and continuum-based, and the yield function includes a hydrostatic stress term to take volume changes in the foam into account. A thorough presentation of the model and the basis for the implementation are given in the following.

It is assumed that the elastic strains are small compared with the plastic strains, and an additive decomposition of the rate-of-deformation tensor $\mathbf{D}$ into elastic and plastic parts is adopted

$$\mathbf{D} = \mathbf{D}^e + \mathbf{D}^p \tag{1}$$

where the indices e and p denote the elastic and plastic parts, respectively. The hypoelastic relation expresses the Jaumann rate $\boldsymbol{\sigma}^{\nabla J}$ of the Cauchy stress tensor $\boldsymbol{\sigma}$ in terms of the elastic rate-of-deformation tensor $\mathbf{D}^e$ in the form

$$\boldsymbol{\sigma}^{\nabla J} = Ktr(\mathbf{D}^e)\mathbf{I} + 2G\mathbf{D}^{e,\mathrm{dev}} \tag{2}$$

where K is the bulk modulus, G is the shear modulus, $\mathbf{I}$ is the second-order unit tensor, and $\mathbf{D}^{e,\mathrm{dev}}$ is the deviatoric part of the elastic rate-of-deformation tensor,

$$\mathbf{D}^{e,\mathrm{dev}} = \mathbf{D}^e - \frac{1}{3}tr\left(\mathbf{D}^e\right)\mathbf{I} \tag{3}$$

The Jaumann rate of the Cauchy stress tensor is given as

$$\boldsymbol{\sigma}^{\nabla J} = \frac{D\boldsymbol{\sigma}}{Dt} - \mathbf{W}\cdot\boldsymbol{\sigma} - \boldsymbol{\sigma}\cdot\mathbf{W}^T \tag{4}$$

In Eqn. (4), $D\boldsymbol{\sigma}/Dt$ is the material time derivative of the Cauchy stress tensor, and $\mathbf{W}$ is the spin tensor.

The yield function Φ is defined by

$$\Phi = \hat{\sigma} - Y \le 0 \tag{5}$$

and the yield stress Y can be expressed as

$$Y = \sigma_p + R(\hat{\varepsilon}) \tag{6}$$

where σ_p is the foam plateau stress, $R(\hat{\varepsilon})$ represents the strain hardening and $\hat{\varepsilon}$ is the equivalent strain. The equivalent stress, $\hat{\sigma}$, is given by (Deshpande and Fleck 2000)

$$\hat{\sigma}^2 = \frac{1}{\left[1+(\alpha/3)^2\right]}\left[\sigma_e^2 + \alpha^2\sigma_m^2\right] \tag{7}$$

where σ_e is the von Mises effective stress, and σ_{m} and $\boldsymbol{\sigma}^{\mathrm{dev}}$ are respectively the mean and deviatoric stresses

$$\sigma_e = \sqrt{\frac{3}{2}\boldsymbol{\sigma}^{\mathrm{dev}} : \boldsymbol{\sigma}^{\mathrm{dev}}}\ ,\ \sigma_{\mathrm{m}} = \frac{1}{3}\mathrm{tr}(\boldsymbol{\sigma}),\ \boldsymbol{\sigma}^{\mathrm{dev}} = \boldsymbol{\sigma} - \frac{1}{3}tr(\boldsymbol{\sigma})\mathbf{I} = \boldsymbol{\sigma} - \sigma_{\mathrm{m}}\mathbf{I} \tag{8}$$

The parameter α defines the shape of the yield surface.

The plastic rate-of-deformation and the equivalent strain rate are defined by the associated flow rule (Lemaitre and Chaboche 1990)

$$\mathbf{D}^p = \dot{\lambda}\frac{\partial \Phi}{\partial \boldsymbol{\sigma}} \tag{9}$$

$$\dot{\hat{\varepsilon}} = -\dot{\lambda}\frac{\partial \Phi}{\partial R} = \dot{\lambda} \tag{10}$$

where $\dot{\lambda}$ is the plastic rate parameter. The loading-unloading conditions can be stated as

$$\Phi \le 0, \quad \dot{\lambda} \ge 0, \quad \dot{\lambda}\Phi \equiv 0 \tag{11}$$

which assure that (1) the stress state lies on or within the yield surface, (2) the plastic rate parameter is non-negative, and (3) the stress lies on the yield surface during plastic loading.

The plastic strain rate can be expressed as

$$\mathbf{D}^p = \dot{\lambda}\frac{\partial \Phi}{\partial \boldsymbol{\sigma}} = \dot{\hat{\varepsilon}}\frac{\partial \Phi}{\partial \sigma_e}\frac{\partial \sigma_e}{\partial \boldsymbol{\sigma}} + \dot{\hat{\varepsilon}}\frac{\partial \Phi}{\partial \sigma_m}\frac{\partial \sigma_m}{\partial \boldsymbol{\sigma}} \tag{12}$$

where,

$$\frac{\partial \Phi}{\partial \sigma_e} = \frac{1}{1+(\alpha/3)^2}\frac{\sigma_e}{\hat{\sigma}}, \qquad \frac{\partial \Phi}{\partial \sigma_m} = \frac{\alpha^2}{1+(\alpha/3)^2}\frac{\sigma_m}{\hat{\sigma}} \tag{13}$$

$$\frac{\partial \sigma_e}{\partial \boldsymbol{\sigma}} = \frac{3}{2}\frac{\boldsymbol{\sigma}^{\mathrm{dev}}}{\sigma_e} = \mathbf{n}, \qquad \frac{\partial \sigma_m}{\partial \boldsymbol{\sigma}} = \frac{1}{3}\mathbf{I} \tag{14}$$

Here, **n** is the normal vector.

The von Mises effective plastic strain rate is

$$\dot{\varepsilon}_e \equiv \sqrt{\frac{2}{3}\mathbf{D}^{\mathrm{p,dev}} : \mathbf{D}^{\mathrm{p,dev}}} = \frac{\dot{\hat{\varepsilon}}}{1+(\alpha/3)^2}\frac{\sigma_e}{\hat{\sigma}} = \dot{\hat{\varepsilon}}\frac{\partial \Phi}{\partial \sigma_e} \tag{15}$$

and the volumetric plastic strain rate is here defined as

$$\dot{\varepsilon}_m \equiv tr\left(\mathbf{D}^{\mathrm{p}}\right) = \frac{\alpha^2\dot{\hat{\varepsilon}}}{1+(\alpha/3)^2}\frac{\sigma_m}{\hat{\sigma}} = \dot{\hat{\varepsilon}}\frac{\partial \Phi}{\partial \sigma_m} \tag{16}$$

It is accordingly possible to split the plastic strain rate into deviatoric and hydrostatic parts in the following simple form:

$$\mathbf{D}^{\mathrm{p}} = \dot{\varepsilon}_e\mathbf{n} + \frac{1}{3}\dot{\varepsilon}_m\mathbf{I} \tag{17}$$

Combination of the equations above gives the equivalent strain rate $\dot{\hat{\varepsilon}}$ expressed explicitly in terms of $\dot{\varepsilon}_e$ and $\dot{\varepsilon}_m$:

$$\dot{\hat{\varepsilon}}^2 = \left[1+\left(\frac{\alpha}{3}\right)^2\right]\left(\dot{\varepsilon}_e{}^2 + \frac{1}{\alpha^2}\dot{\varepsilon}_m{}^2\right) \tag{18}$$

The yield criterion in Eqn. (5) is used with the following definition of the parameter α (Deshpande and Fleck 2000):

$$\alpha^2 = \frac{9}{2}\frac{(1-2\nu^p)}{(1+\nu^p)} \tag{19}$$

where ν^p is the plastic coefficient of contraction. If $\alpha^2 = 4.5$, there will be no lateral plastic deformation resulting from uniaxial compression, which means that the measured engineering stress is identical to the true stress. The values of α^2 should be limited within the range of $0 \le \alpha^2 \le 4.5$ to be physically admissible. The upper limit corresponds to zero plastic coefficient of contraction, while the lower limit corresponds to the von Mises criterion.

Numerical Implementation Procedure

The constitutive equations presented in the previous section have been implemented in the explicit finite element program LS-DYNA. The integration algorithm (or stress-update scheme) for the rate constitutive equations is developed next. The adopted stress-update algorithm is based on the work of Aravas (1987) for pressure-dependent materials, while a general reference to Belytschko et al. (2000) is made for more details on stress-update algorithms.

Assume that the stress tensor $\boldsymbol{\sigma}_{\mathrm{n}}$ and the effective plastic strain $\hat{\varepsilon}_{\mathrm{n}}$ at time t_{n} have been computed, and, in addition, that the rate-of-deformation tensor $\mathbf{D}_{\mathrm{n+1/2}}$ and the spin tensor $\mathbf{W}_{\mathrm{n+1/2}}$ at time $t_{\mathrm{n+1/2}} = t_{\mathrm{n}} + \Delta t_{\mathrm{n+1}}/2$ are known from the finite element solution. The strain increment $\Delta\boldsymbol{\varepsilon}_{\mathrm{n+1}}$ occurring during the time step $\Delta t_{\mathrm{n+1}} = t_{\mathrm{n+1}} - t_{\mathrm{n}}$ is then calculated by

$$\Delta\boldsymbol{\varepsilon}_{\mathrm{n+1}} = \mathbf{D}_{\mathrm{n+1/2}}\,\Delta t_{\mathrm{n+1}} \tag{20}$$

and the task is to determine the updated variables $\boldsymbol{\sigma}_{\mathrm{n+1}}$ and $\hat{\varepsilon}_{\mathrm{n+1}}$ at time $t_{\mathrm{n+1}}$.

A trial stress state is first calculated assuming the increment purely elastic, i.e. (Crisfield 1997, Hallquist 1998)

$$\boldsymbol{\sigma}^{tr}_{\mathrm{n+1}} = \boldsymbol{\sigma}_{\mathrm{n}} + \Delta t_{\mathrm{n+1}}\left(\mathbf{W}_{\mathrm{n+1/2}}\boldsymbol{\sigma}_{\mathrm{n}} + \boldsymbol{\sigma}_{\mathrm{n}}\mathbf{W}^{\mathrm{T}}_{\mathrm{n+1/2}}\right) + Ktr(\Delta\boldsymbol{\varepsilon}_{\mathrm{n+1}})\mathbf{I} + 2G\Delta\boldsymbol{\varepsilon}^{\mathrm{dev}}_{\mathrm{n+1}} \tag{21}$$

The transformation of the stress tensor $\boldsymbol{\sigma}_n$ at t_n is necessary to correctly account for the rigid body rotation of the material during the time step Δt_{n+1}. It is then checked if the assumption of an elastic time step is correct or if the trial stress leads to plasticity:

$$\Phi^{tr}_{\mathrm{n+1}} = \hat{\sigma}^{tr}_{\mathrm{n+1}} - Y_n \le 0 \quad \Rightarrow \quad \text{elastic step} \quad \Rightarrow \quad \begin{cases} \boldsymbol{\sigma}_{\mathrm{n+1}} = \boldsymbol{\sigma}^{tr}_{\mathrm{n+1}} \\ \hat{\varepsilon}_{\mathrm{n+1}} = \hat{\varepsilon}_{\mathrm{n}} \end{cases} \tag{22}$$

$$\Phi^{tr}_{\mathrm{n+1}} = \hat{\sigma}^{tr}_{\mathrm{n+1}} - Y_n > 0 \quad \Rightarrow \quad \text{plastic step} \quad \Rightarrow \quad \text{return map} \tag{23}$$

Here, the trial value of the equivalent stress in the current step, and the yield stress in the previous step, can be written as

$$\hat{\sigma}^{tr}_{\mathrm{n+1}} = \sqrt{\frac{1}{1+(\alpha/3)^2}\left[\left(\sigma^{tr}_{e,\mathrm{n+1}}\right)^2 + \alpha^2\left(\sigma^{tr}_{m,\mathrm{n+1}}\right)^2\right]} \tag{24}$$

and

$$Y_{\mathrm{n}} = Y\left(\hat{\varepsilon}_{\mathrm{n}}\right) = \sigma_p + R\left(\hat{\varepsilon}_{\mathrm{n}}\right) \tag{25}$$

For a plastic step, an iterative radial return algorithm is used to re-establish consistency. The stress at $t_{\mathrm{n+1}}$ is calculated as

$$\boldsymbol{\sigma}_{\mathrm{n+1}} = \boldsymbol{\sigma}^{tr}_{\mathrm{n+1}} - Ktr(\Delta\boldsymbol{\varepsilon}^{p}_{\mathrm{n+1}})\mathbf{I} - 2G\Delta\boldsymbol{\varepsilon}^{p,\mathrm{dev}}_{\mathrm{n+1}} = \boldsymbol{\sigma}^{tr}_{\mathrm{n+1}} - K\Delta\varepsilon_{m,\mathrm{n+1}}\mathbf{I} - 2G\Delta\varepsilon_{e,\mathrm{n+1}}\mathbf{n}_{\mathrm{n+1}} \tag{26}$$

where $\Delta\varepsilon_{m,\mathrm{n+1}}$ and $\Delta\varepsilon_{e,\mathrm{n+1}}$ are increments of the volumetric and von Mises effective plastic strains, respectively. The normal vector $\mathbf{n}_{\mathrm{n+1}}$ reads

$$\mathbf{n}_{\mathrm{n+1}} = \frac{3}{2}\frac{\boldsymbol{\sigma}^{\mathrm{dev}}_{\mathrm{n+1}}}{\sigma_{e,\mathrm{n+1}}} = \frac{3}{2}\frac{\boldsymbol{\sigma}^{\mathrm{dev,tr}}_{\mathrm{n+1}}}{\sigma^{\mathrm{tr}}_{e,\mathrm{n+1}}} \tag{27}$$

where the latter equality is due to the spherical shape of the flow potential in deviatoric stress space (Aravas 1987).

Consistency at t_{n+1} requires that

$$\Phi_{n+1} = \hat{\sigma}_{n+1} - Y\left(\hat{\varepsilon}_{n+1}\right) = 0 \quad \Rightarrow \quad \hat{\sigma}_{n+1} = Y\left(\hat{\varepsilon}_{n+1}\right) \tag{28}$$

where

$$\hat{\varepsilon}_{n+1} = \hat{\varepsilon}_n + \Delta\hat{\varepsilon}_{n+1} \tag{29}$$

Here, $\Delta\hat{\varepsilon}_{n+1}$ is the increment of the equivalent plastic strain. From Eqns. (15), (16), and (28), the increments in the deviatoric and volumetric strains can be written as

$$\Delta\varepsilon_{e,n+1} = \Delta\hat{\varepsilon}_{n+1}\frac{1}{1+(\alpha/3)^2}\frac{\sigma_{e,n+1}}{Y_{n+1}} \tag{30}$$

$$\Delta\varepsilon_{m,n+1} = \Delta\hat{\varepsilon}_{n+1}\frac{\alpha^2}{1+(\alpha/3)^2}\frac{\sigma_{m,n+1}}{Y_{n+1}} \tag{31}$$

where

$$\hat{\sigma}_{n+1} = Y_{n+1} = \sigma_p + R\left(\hat{\varepsilon}_{n+1}\right) \tag{32}$$

Projection of $\boldsymbol{\sigma}_{n+1}$ onto $\mathbf{I}$ and $\mathbf{n}_{n+1}$ makes it possible to divide the stress into a deviatoric and hydrostatic parts (Aravas 1987):

$$\sigma_{m,n+1} = \sigma^{tr}_{m,n+1} - K\Delta\hat{\varepsilon}_{m,n+1} \quad \Rightarrow \quad \sigma_{m,n+1} = \frac{\sigma^{tr}_{m,n+1}}{1+\dfrac{K\Delta\hat{\varepsilon}_{n+1}\alpha^2}{\left(1+(\alpha/3)^2\right)Y_{n+1}}} \tag{33}$$

$$\sigma_{e,n+1} = \sigma^{tr}_{e,n+1} - 3G\Delta\hat{\varepsilon}_{e,n+1} \quad \Rightarrow \quad \sigma_{e,n+1} = \frac{\sigma^{tr}_{e,n+1}}{1+\dfrac{3G\Delta\hat{\varepsilon}_{n+1}}{\left(1+(\alpha/3)^2\right)Y_{n+1}}} \tag{34}$$

The equation that remains to be solved is the yield condition at t_{n+1}:

$$\Phi_{n+1}\left(\Delta\hat{\varepsilon}_{n+1}\right) = \hat{\sigma}_{n+1} - Y_{n+1} = \sqrt{\frac{1}{1+(\alpha/3)^2}\left[\left(\sigma_{e,n+1}\right)^2 + \alpha^2\left(\sigma_{m,n+1}\right)^2\right]} - Y_{n+1} = 0 \tag{35}$$

where the unknown quantity is $\Delta\hat{\varepsilon}_{n+1}$. Eqn. (35) is solved using Newton's method,

$$\Phi_{n+1}^{(k+1)} = \Phi_{n+1}^{(k)} + \left(\frac{\partial \Phi}{\partial \Delta \hat{\varepsilon}}\right)_{n+1}^{(k)} \delta \Delta \hat{\varepsilon}_{n+1}^{(k)} = 0 \quad \Rightarrow \quad \delta \Delta \hat{\varepsilon}_{n+1}^{(k)} = -\frac{\Phi_{n+1}^{(k)}}{\left(\frac{\partial \Phi}{\partial \Delta \hat{\varepsilon}}\right)_{n+1}^{(k)}}$$
$$\Delta \hat{\varepsilon}_{n+1}^{(k+1)} = \Delta \hat{\varepsilon}_{n+1}^{(k)} + \delta \Delta \hat{\varepsilon}_{n+1}^{(k)} \tag{36}$$

and the stress tensor, $\boldsymbol{\sigma}_{n+1}$, is then obtained by Eqn. (26). $\left(\frac{\partial \Phi}{\partial \Delta \hat{\varepsilon}}\right)_{n+1}^{(k)}$ can be derived analytically from the yield function, but it is also possible to express it numerically:

$$\left(\frac{\partial \Phi}{\partial \Delta \hat{\varepsilon}}\right)_{n+1}^{(k)} \approx \frac{\Phi_{n+1}^{(k)} - \Phi_{n+1}^{(k-1)}}{\Delta \hat{\varepsilon}_{n+1}^{(k)} - \Delta \hat{\varepsilon}_{n+1}^{(k-1)}} \tag{37}$$

Statistical Variation

The different size and uneven distribution of the pores lead to a density variation in the foam. It was attempted to model the variation in properties without modeling the pore structure, but instead introducing an initial statistical variation of the material properties. As the material properties for foam generally are functions of the foam density, each element can be given a different density, and the material parameters can consequently be calculated from the density. A hardening model where it is possible to include the variation of foam density was suggested by Hanssen et al. (2002), and a slightly modified version of this was used in the implemented model (Reyes et al. 2003):

$$Y = \sigma_p + R(\hat{\varepsilon}) = \sigma_p + \gamma \frac{\hat{\varepsilon}}{\varepsilon_D} + \alpha_2 \ln\left(\frac{1}{1-(\hat{\varepsilon}/\varepsilon_D)^{\beta}}\right) \tag{38}$$

where, σ_p, α_2, γ, β, and ε_D are the material parameters. The material properties, σ_p, α_2, γ, and β, can be expressed as functions of the foam density (Hanssen et al. 2002):

$$\left\{\sigma_p, \alpha_2, \gamma, \frac{1}{\beta}\right\} = C_0 + C_1\left(\frac{\rho_f}{\rho_{f0}}\right)^n \tag{39}$$

where C_0, C_1, and n are constants.

The compaction strain ε_D was defined as (Reyes et al. 2003)

$$\varepsilon_D = -\frac{9+\alpha^2}{3\alpha^2}\ln\left(\frac{\rho_f}{\rho_{f0}}\right) \tag{40}$$

As the material parameters in the hardening curve can all be considered functions of the foam density, a statistical variation of the foam density was introduced, i.e. the mean value and

standard deviation must be given as input parameters. In the initialization of the analysis, each element is given a foam density with a normal (Gaussian) probability distribution. The material parameters are calculated from the density for each element, using Eqns. (39) and (40). A function, "Gasdev" (Press et al. 1986-1992), was used to generate random deviates with a normal (Gaussian) probability distribution. When each element is given a random density in the beginning of the analysis, one numerical simulation will be different from the next. Hence, one analysis can be an "extreme" case that is not likely to happen. Several analyses should therefore be carried out to make sure that the response is of a wanted probability. Figure 1 shows an example of how the density is distributed in a foam specimen.

The material constants, C_0, C_1, and n should be calibrated to Eqn. (39) when using the option with statistical variation of the parameters, as the material constants all depend on the foam density. However, this requires that a larger experimental database is available. Hanssen et al. (2002) pointed out that the fit to Eqn. (39) is best for the plateau stress while there is some deviation for the other parameters. Nevertheless, as the main goal is to introduce a variation in the material parameters, the use of Eqn. (39) seems reasonable.

Fracture

Two simple fracture criteria were implemented in the model. As fracture is often modeled in FEM-analyses by removing (eroding) elements when they reach a critical value of strain, one possible fracture criterion was to use the volumetric strain ε_m as a measure for when an element should be eroded:

$$\text{If } \varepsilon_m \geq \varepsilon_{\text{cr}} \quad \Rightarrow \quad \text{erosion of element} \tag{41}$$

where ε_{cr} is the critical strain. Eqn. (41) was implemented in the subroutine, and the criterion will be referred to as "fr1" in the following.

In addition, a second fracture criterion was implemented. As only hydrostatic deformation is included in the first criterion, and it is natural to assume that also deviatoric deformation can cause fracture, a criterion where the principal stress is used for evaluation of fracture was also

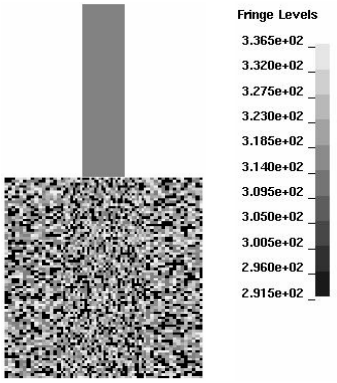

Figure 1 Distribution of density for analysis with statistical variation, $\rho = 0.314 \pm 0.0225$ g/cm^3

implemented. The criterion is based on erosion of elements when the maximum principal stress reaches a critical value:

$$\text{If } \sigma_1 \geq \sigma_{\text{cr}} \quad \Rightarrow \quad \text{erosion of element} \tag{42}$$

where σ_{cr} is the critical stress. As the tensile failure stress was approximately equal to the initial plateau stress in compression (Hanssen et al. 2002), it can be used as a critical value of the principal stress, i.e. $\sigma_{\text{cr}} = \sigma_p$. However, because of spurious noise produced by contact forces and elastic stress waves which are initiated when an element is eroded, the stress levels in the elements can at times be higher than the critical stress, although these should not necessarily cause fracture. To avoid premature erosion of elements, an energy-based criterion was established from Eqn. (42), motivated by a fracture criterion for metals due to Cockcroft and Latham (1968). The fracture criterion reads:

$$\text{If} \quad \int_0^{\hat{\varepsilon}} H\left(\sigma_1 - \sigma_{cr}\right)\sigma_1 d\hat{\varepsilon} \geq C \quad \Rightarrow \quad \text{erosion of element} \tag{43}$$

where, *H(x)* is defined as

$$H\left(x\right) = \begin{cases} 1 & \text{if} \quad x \geq 0 \\ 0 & \text{if} \quad x < 0 \end{cases} \tag{44}$$

Eqn. (43) was implemented in the subroutine, and the criterion will be referred to as “fr2” in the following. Be aware that the critical value *C* can be problem dependent and has thus to be selected based on experience or validation studies using experimental data.

Model Verification

As mentioned in the introduction, the model verification is thoroughly reported by Reyes et al. (2003). However, some of the results will be presented briefly here to show the correlation between analyses and experiments.

Several verification tests were carried out by Hanssen et al. (2002). This experimental program included indentation tests called “Mval 1” and diagonal loading called “Mval 2”, and some of the results of these two tests will be presented in the following. The verification study also included uniaxial and hydrostatic compression tests, but the results from these will not be discussed here. However, it is worth mentioning that the uniaxial compression tests were predicted by the analyses with very good accuracy, while the hydrostatic compression analyses deviated significantly from the experiments. Yet, the theoretical behavior resulting from Eqns. (7), (18) and (38) were predicted (Reyes et al. 2003).

The test specimens of “Mval1” and “Mval2” were cubic with dimensions 70x70x70 mm^3. Because the plastic coefficient of compression was assumed zero, plane strain conditions could be applied, and both 2D and 3D analyses were carried out. For the 3D analyses, it was necessary to use a fully integrated S/R solid element, while the default eight-node brick element of LS-DYNA was applied with one point reduced integration scheme for the 2D analyses as much finer meshes could be used. The stiffness based hourglass control #5 in LS-DYNA was used in order

to avoid hourglassing. The tests were loaded quasi-statically, and the load was applied through a rigid body which was given the following prescribed velocity field to ensure quasi-static loading

$$v(t) = \frac{\pi}{\pi - 2} \cdot \frac{d_{\max}}{T} \left[1 - \cos\left(\frac{\pi}{2T} \cdot t \right) \right] \tag{45}$$

Here, T is the total duration of the loading, $d_{\max}$ is the final displacement. When integrated from $t = 0$ to $t = T$, Eqn. (45) yields $d_{\max}$, and when differentiated with respect to time, the initial acceleration equals zero. The applied velocity and pressure fields should ensure that the loading takes place gradually and that unnecessary dynamics in the numerical solution are avoided (Ilstad 1999). The termination time T was 0.1 s.

Mesh sensitivity studies of the 2D analyses were carried out, and the solution converged for a model of 2574 ("Mval1") and 1600 ("Mval2") elements.

"Mval 1"

3D analyses of "Mval1" where fracture was neglected were carried out, in addition to analyses with the two fracture criteria and analyses with statistical variation of the foam density. Figure 2 shows how the indentation tests behaved in the experiments, and how the analyses without fracture were not able to predict this behavior. The deformation behavior of the analyses including fracture (both "fr1" and "fr2"), and statistical variation of density are shown in Figure 3. As one can see, the analyses with "fr2" are very similar to the physical tests. Figure 4 shows the force-displacement curves from the analyses and experiments, and the force-displacement behavior is very well predicted by the analyses with "fr2". The force levels are overestimated in the analyses where fracture is neglected, and in the analyses with "fr1". It is also obvious that the statistical variation of density does not have a great influence on the force-displacement curves.

"Mval 2"

Both 2D and 3D analyses of "Mval 2" were carried out, and the deformation behavior and force-displacement curves from both experiments and analyses are shown in Figure 5. As one can see, both 2D and 3D models predicted the behavior in the physical tests with good accuracy.

Correlation between analyses and experiments

Correlation plots between mean loads from analyses and experiments are shown in Figure 6 for both "Mval1" and "Mval2". Included in the figure are also results from the uniaxial compression tests (called "Cal1"). As one can see, there is a very good correlation for "Cal1", "Mval2" and "Mval1" with "fr2".

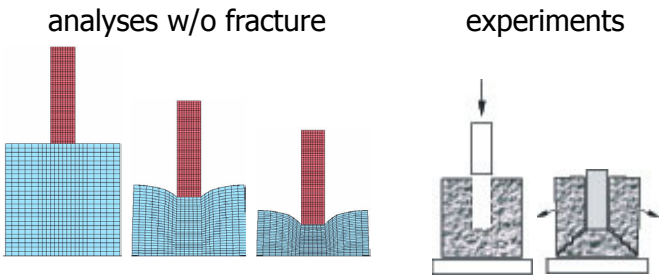

Figure 2 Deformation behavior of “Mval 1”

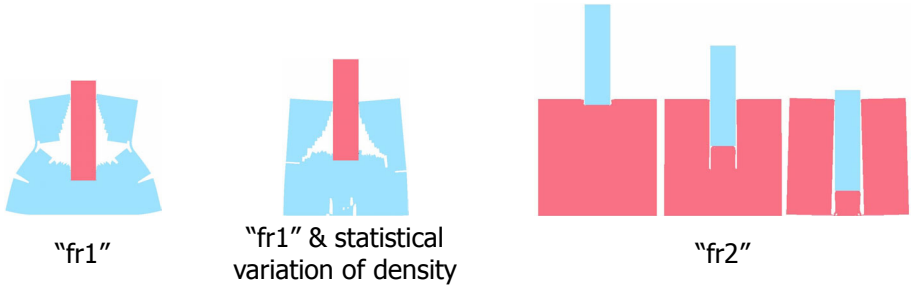

Figure 3 Deformation behavior of “Mval 1”, plane strain model

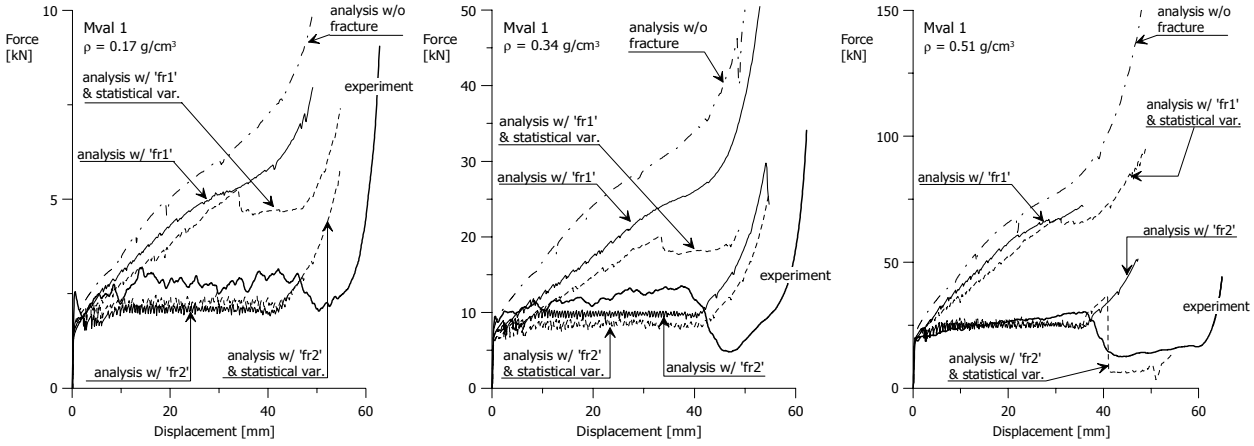

Figure 4 Force-displacement plots for indentation test (“Mval 1”): experiments and different analyses

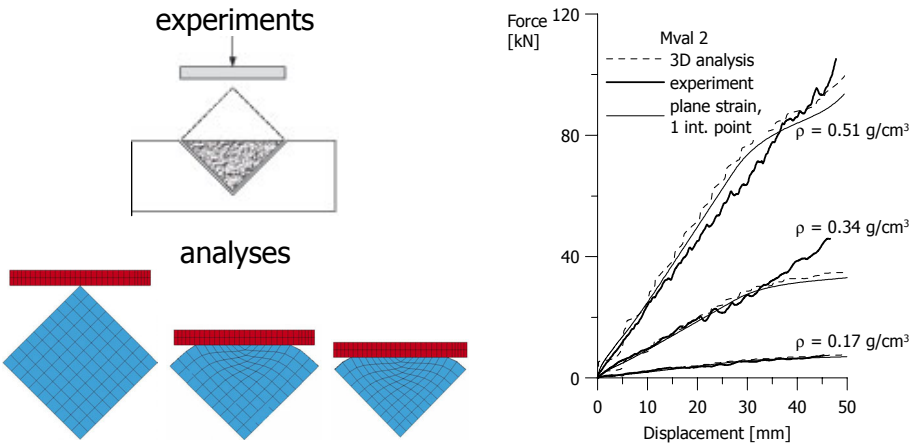

Figure 5 Deformation behavior and force-displacement curves of "Mval 2"

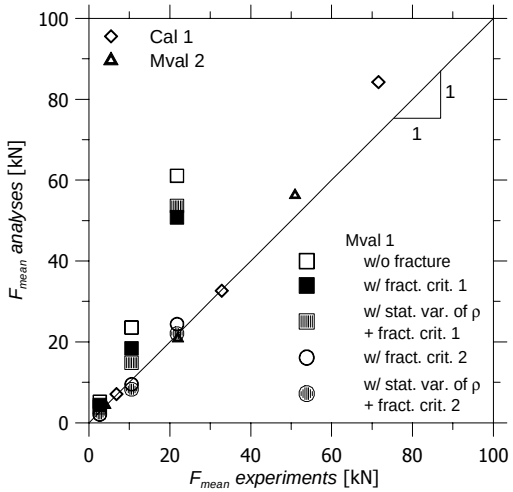

Figure 6 Correlation between mean loads from numerical analyses and experiments

Concluding Remarks

The foam model suggested by Deshpande and Fleck has successfully been implemented in LS-DYNA, and two simple fracture criteria and the possibility to include statistical variation of density were incorporated in the model. For the indentation test, a stress-based fracture criterion gave the best results in comparison with the physical tests, and these numerical analyses together with the analyses of the other verification tests were able to predict the behavior in the experiments with good accuracy. Taking statistical variation of density into account did not have a great effect on the behavior. The results from the present project are promising, as the implemented model is efficient, robust, and able to predict the observed behavior in verification experiments. At present, a version of the model containing one of the fracture criteria (the strain-based) and without the possibility of statistical variation of density is available in version 970 of LS-DYNA.

Acknowledgements

The present project has been carried out with financial support from the Faculty of Engineering Science and Technology, NTNU and the Norwegian Research Council.

References

Aravas, N., "On the numerical integration of a class of pressure-dependent plasticity models", p1395-1416, International Journal for Numerical Methods in Engineering 24 (1987).

Belytchko, T., Liu, W.K. and Moran, B., "Nonlinear Finite Elements for Continua and Structures" Wiley, Chichester (2000).

Cockcroft, M.G. and Latham, D.J., "Ductility and the Workability of Metals", p33-39, Journal of the institute of metals 96 (1968).

Crisfield, M.A., "Non-linear Finite Element Analysis of Solids and Structures. Volume 2: Advanced Topics" John Wiley & Sons Ltd., West Sussex (1997).

Daxner, T., Böhm, H.J. and Rammerstorfer, F.G., "Mesoscopic simulation of inhomogeneous metallic foams with respect to energy absorption", p61-69, Computational Materials Science 16 (1999).

Deshpande, V.S. and Fleck, N.A., "Isotropic models for metallic foams", p1253-1283, Journal of the Mechanics and Physics of Solids 48 (2000).

Ehlers, W., "Metalschäume - Metal foams" Report No. 99-II-6. Institut für Mechanik, Bauwesen (1999).

Gradinger, R. and Rammerstorfer, F.G., "On the influence of meso-inhomogeneities on the crush worthiness of metal foams", p143-148, Acta Materialia 47 (1) (1999).

Hallquist, J.O., "Theoretical Manual" Livermore Software Technology Corporation, California (1998).

Hanssen, A.G., Hopperstad, O.S., Langseth, M. and Ilstad, H., "Validation of constitutive models applicable to aluminium foams", p359-406, International Journal of Mechanical Sciences 44 (2002).

Ilstad, H., "Validation of Numerical Collapse Behaviour of Thin-Walled Corrugated Panels" Doctoral Thesis. Norwegian University of Science and Technology, Trondheim (1999).

Lemaitre, J. and Chaboche, J.-L., "Mechanics of solid materials" Cambridge University Press, Cambridge (1990).

Meguid, S.A., Cheon, S.S. and El-Abbasi, N., "FE modelling of deformation localization in metallic foams", p631-643, Finite elements in analysis and design 38 (2002).

Miller, R.E., "A continuum plasticity model for constitutive and indentation behaviour of foamed metals", p729-754, International Journal of Mechanical Sciences 42 (2000).

Press, W.H., Flannery, B.P., Teukolsky, S.A. and Vetterling, W.T., "Numerical recipes in Fortran 77: The art of scientific computing" Cambridge University Press, Cambridge (1986-1992).

Reyes, A., Hopperstad, O.S., Berstad, T., Hanssen, A.G. and Langseth, M., "Constitutive modeling of aluminum foam including fracture and statistical variation of density", p815-835, European Journal of Mechanics A/Solids 22 (6) (2003).

Schreyer, H.L., Zuo, Q.H. and Maji, A.K., "Anisotropic Plasticity Model for Foams and Honeycombs", p1913-1930, Journal of Engineering Mechanics 120 (9) (1994).

Zhang, J., Lin, Z., Wong, A., Kikuchi, N., Li, V.C., Yee, A.F. and Nusholtz, G.S., "Constitutive Modeling and Material Characterization of Polymeric Foams", p284-291, Journal of Engineering Materials And Technology 119 (1997).